Article

Structure

Chain Assembly and Disassembly Processes Differently Affect the Conformational Space of Ubiquitin Chains

Graphical Abstract

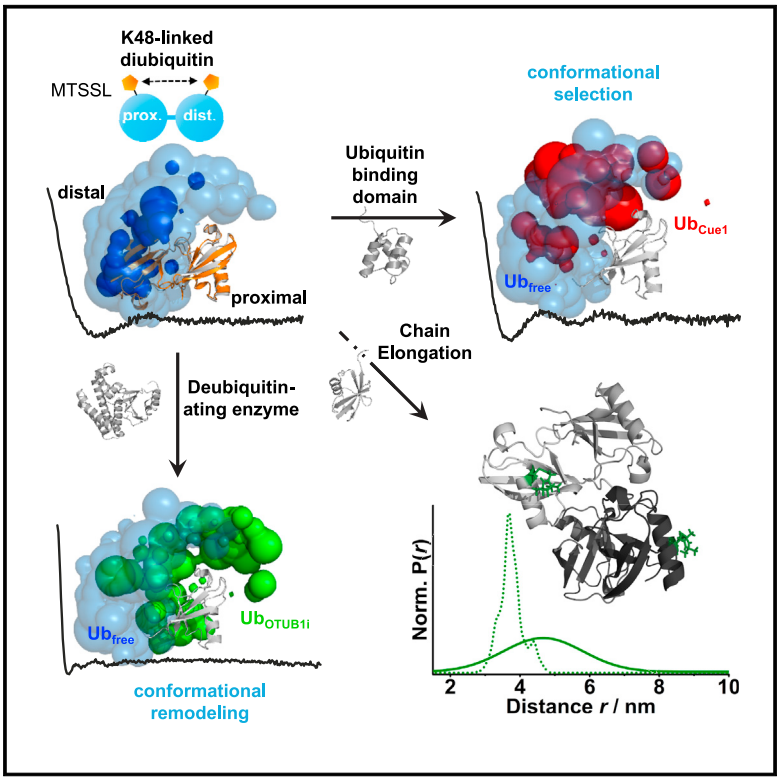

Authors

Andreas Kniss, Denise Schuetz, Sina Kazemi, ..., Thomas Sommer, Thomas F. Prisner, Volker Dötsch

Correspondence

prisner@chemie.uni-frankfurt.de (T.F.P.), vdoetsch@em.uni-frankfurt.de (V.D.)

In Brief

In this work, Kniss et al. provide a comprehensive analysis of the conformational space of K48-linked ubiquitin chains and how chain conformations and flexibility are altered during assembly and disassembly of ubiquitin signals.

Highlights

- K48-linked diubiquitin samples a broad conformational space
- Cue1 uses conformational selection to support the chain elongation process
- The linkage-specific DUB OTUB1 remodels the conformational distribution
- Elongation to tetraubiquitin does not restrict but increases the conformational space

Kniss et al., 2018, Structure *26*, 249–258
February 6, 2018
https://doi.org/10.1016/j.str.2017.12.011

CellPress

Structure
Article

Chain Assembly and Disassembly Processes Differently Affect the Conformational Space of Ubiquitin Chains

Andreas Kniss,[1,8] Denise Schuetz,[2,8] Sina Kazemi,[1,4] Lukas Pluska,[3] Philipp E. Spindler,[2] Vladimir V. Rogov,[1] Koraljka Husnjak,[5] Ivan Dikic,[5] Peter Güntert,[1,6] Thomas Sommer,[3,7] Thomas F. Prisner,[2,*] and Volker Dötsch[1,9,*]
[1]Institute of Biophysical Chemistry and Center for Biomolecular Magnetic Resonance, Goethe University, Max-von-Laue Strasse 9, 60438 Frankfurt am Main, Germany
[2]Institute of Physical and Theoretical Chemistry and Center for Biomolecular Magnetic Resonance, Goethe University, Max-von-Laue Strasse 7, 60438 Frankfurt am Main, Germany
[3]Max-Delbrück Center for Molecular Medicine in the Helmholtz Association, Robert-Rössle-Strasse 10, 13125 Berlin-Buch, Germany
[4]Frankfurt Institute for Advanced Studies, Goethe University Frankfurt, Ruth-Moufang-Strasse 1, 60438 Frankfurt am Main, Germany
[5]Institute of Biochemistry II, Goethe University Medical School, Theodor-Stern-Kai 7, 60590 Frankfurt, Germany
[6]Laboratory of Physical Chemistry, ETH Zurich, Vladimir-Prelog-Weg 2, 8093 Zurich, Switzerland
[7]Institute for Biology, Humboldt Universität zu Berlin, Invalidenstrasse 43, 10115 Berlin, Germany
[8]These authors contributed equally
[9]Lead Contact
*Correspondence: prisner@chemie.uni-frankfurt.de (T.F.P.), vdoetsch@em.uni-frankfurt.de (V.D.)
https://doi.org/10.1016/j.str.2017.12.011

SUMMARY

Ubiquitination is the most versatile posttranslational modification. The information is encoded by linkage type as well as chain length, which are translated by ubiquitin binding domains into specific signaling events. Chain topology determines the conformational space of a ubiquitin chain and adds an additional regulatory layer to this ubiquitin code. In particular, processes that modify chain length will be affected by chain conformations as they require access to the elongation or cleavage sites. We investigated conformational distributions in the context of chain elongation and disassembly using pulsed electron-electron double resonance spectroscopy in combination with molecular modeling. Analysis of the conformational space of diubiquitin revealed conformational selection or remodeling as mechanisms for chain recognition during elongation or hydrolysis, respectively. Chain elongation to tetraubiquitin increases the sampled conformational space, suggesting that a high intrinsic flexibility of K48-linked chains may contribute to efficient proteasomal degradation.

INTRODUCTION

Ubiquitination regulates a diverse array of cellular signaling processes next to its key function of mediating proteasomal degradation. A prerequisite for the specific outcome of ubiquitin signaling is the discrimination of the differently linked ubiquitin chains by ubiquitin binding domains (UBDs) (Dikic et al., 2009). They recognize either the canonical hydrophobic patch of ubiquitin or the linkage itself, and distinct ubiquitin chain conformations have been suggested as an additional regulatory layer in signal transduction. Next to this classical role, UBDs additionally exert a wide array of regulatory functions with some directly implicated in the ubiquitination process itself (von Delbrück et al., 2016). Similar to protein phosphorylation, ubiquitination is reversible, and chains can be specifically hydrolyzed by the action of deubiquitinating enzymes (DUBs) (Komander et al., 2009). Our recent work has shown how the UBD of Cue1 can promote ubiquitin chain elongation within the endoplasmic reticulum-associated degradation (ERAD) process by positioning the growing ubiquitin chain relative to the E2 enzyme, thereby acting in an E4-like fashion as an accelerating factor of chain synthesis (von Delbrück et al., 2016). The current view of the conformation of K48-linked ubiquitin chains is a compact arrangement with the hydrophobic patches sequestered at the inter-domain interface (Hirano et al., 2011; Ryabov and Fushman, 2006; Ye et al., 2012). However, within this spatially dynamic process, the influence of ubiquitin chain conformations has not yet been addressed. In addition, the compact arrangement of K48-linked ubiquitin chains has also been suggested to affect the activity of DUBs (Ye et al., 2012). Therefore, determining the accessible conformational space of ubiquitin chains and how UBDs and DUBs affect the conformational distribution is the key to understanding the full scope of the ubiquitin code.

Previous structural studies mostly applied methods, which are mainly sensitive to short-range interactions yielding snapshots of specific conformations, whereas the whole sampled conformational space and its dependence on chain length remain elusive. For K48-linked tetraubiquitin, the minimal signal for efficient proteasomal degradation (Thrower et al., 2000), a compact structure has been reported (Eddins et al., 2007). Such a compact structure, however, necessitates remodeling of the conformation for efficient recognition at the proteasome by the receptors Rpn10 and Rpn13 (Zhang et al., 2016). We addressed these questions experimentally by analyzing ubiquitin chains of various

length by pulsed electron-electron double resonance (PELDOR, also called DEER) spectroscopy (Jeschke, 2012; Milov et al., 1981, 1984). PELDOR is a method for measuring long-range distances (1.8 to 6–10 nm) and their distribution in spin-labeled macromolecules. We used the recently developed seven-pulse Carr-Purcell (CP) PELDOR sequence (Spindler et al., 2015), which provides an increased accuracy of the observable distance distributions, especially for long distances with broad distributions. In combination with the small size of the attached spin labels, PELDOR is optimally suited for the investigation of the conformational space of flexible multi-domain proteins. Here, we show that diubiquitin adopts a wide conformational space that gets even more enlarged by further chain elongation. We further investigate chain recognition mechanisms by the UBD of Cue1 and DUBs.

RESULTS

Differently Linked Diubiquitins Reveal Specific Conformational Flexibilities

The current model suggests that ubiquitin chains of different linkage types adopt distinct chain conformations, influencing how ubiquitin signals are recognized in the cell. Characterization of conformations and flexibilities of such multi-domain proteins requires the measurement of long-range distance restraints in the nanometer range, which are accessible by PELDOR spectroscopy. Since PELDOR time traces are sensitive to the conformational flexibility of both spin label and protein molecule (Dastvan et al., 2016; Jeschke, 2013; Klose et al., 2012; Polyhach et al., 2010), we used doubly spin-labeled monoubiquitin to assess the inherent intra-ubiquitin conformational flexibility (Figures S1A and S1B). Subsequently, we investigated how different linkage types of diubiquitin chains influence the conformational space by attaching one spin label to each ubiquitin moiety. We fitted the distance distributions for K11-, K48-, and K63-linked diubiquitins with a two-Gaussian model (Figure S1C, Table S1) leading to distance distributions ranging from ~2 to 6 nm (Figure 1A). These measurements confirmed previous results that K11-linked chains adopt dynamic, I44-exposing conformations (Bremm et al., 2010), K63-linked chains adopt extended and open conformations (Alfano et al., 2016), and K48-linked chains show a combination of a narrow with an underlying broader distribution. However, the information content of a single long-range restraint is not sufficient to allow any detailed analysis of conformational distributions since ambiguities of different relative ubiquitin orientations are not resolved.

Conformational Space of K48-Linked Ubiquitin Chains

To go beyond this rather qualitative analysis and to characterize the entire conformational space as well as changes triggered by the interaction with ubiquitin binding proteins, we synthesized five differently spin-labeled K48-linked diubiquitins (Figure 1B). Three of the observed time traces showed a pronounced dipolar oscillation, which dampened directly after the first oscillation yielding broad but bimodal distance distributions (Figures 1C, S1D, and S1E). The remaining two time traces did not show oscillations, characteristic of an even broader distance distribution. To represent the conformational space available to K48-linked diubiquitin, we calculated 10^6 structural models employing the software CYANA (combined assignment and dynamics algorithm for nuclear magnetic resonance [NMR] applications) (Güntert and Buchner, 2015; Güntert et al., 1997) (Figure S1F) whereby the backbone of the ubiquitins outside the linker regions was kept rigid. In addition, the spin label flexibility was estimated by rotamer libraries at the given positions and single rotamer pairs were selected for each structural model. This resulted in $\sim 3.7 \times 10^5$ models without steric clashes. A normalized combined pseudo probability derived from all five experimental distance distributions, hereafter referred to as combined probability, was used in another filtering step. Each conformation with a combined probability <1% was dropped, yielding a representative structural ensemble of $\sim 1.4 \times 10^5$ models fulfilling all experimental restraints. Out of this ensemble, we chose 3,000 representative models for visualization (Figures S1F and S1G). In these models the position of the distal ubiquitin, with respect to the proximal one, is indicated by a sphere at the center of mass of this ubiquitin moiety (Figure S1H). The size of the spheres shown in Figure 1 represents the combined probability of a certain position of the distal ubiquitin. This calculation resulted in a broad distribution of conformations, however, with distinct highly populated sub-spaces. These sub-spaces contain a large number of orientations comparable with known closed conformations (PDB: 2O6V, Figure 1D; PDB: 2BGF, 2PEA, 3M3J, Figures 1E, S1I, and Movie S1). Nevertheless, also open conformations with accessible hydrophobic patch residues such as PDB: 2PE9, as well as conformations seen in complexes (PDB: 2LVQ, 2LVP), are highly populated (Figures 1E and S1I). This suggests that only conformational selection out of this pool of highly populated conformations is necessary for ubiquitin binding. Compact structures with accessible hydrophobic patches (PDB: 3NS8 and 3AUL, Figures 1E and S1I) are located in less probable regions. A conformation as seen in complex with the K48-specific UBD UBA2 is found to be possible (PDB: 1ZO6, Figures 1E and S1I), but less probable, for free K48-linked diubiquitin.

To understand how conformational distributions are influenced by the existence of additional ubiquitin moieties, we investigated the conformational space of tri- and tetraubiquitin carrying spin labels in both the proximal and the distal moiety (Figure 2A). The elongation to triubiquitin increases the sampled conformational space leading to a broadening of the distance distribution with respect to diubiquitin (Figures 2B and S2A–S2K). To evaluate whether the compact arrangement of tetraubiquitin seen in the crystal structure PDB: 2O6V is the predominant conformation, we chose three tetraubiquitin variants based on *in silico* spin labeling with the software package MMM2015.2 (Polyhach et al., 2010). The spin label flexibility is hereby taken into account via rotamer libraries. The experimental data for all tetraubiquitin variants can be fitted with a single Gaussian distribution with mean distances between ~3.0 and ~4.9 nm and widths ranging from ~1.5 to 5 nm (Figure 2B and Table S1). This is indicative of a very broad conformational space. Superposition of the experimental time traces and distance distributions with those simulated based on the X-ray structure (PDB: 2O6V) demonstrated that the compact fold is within the conformational space. However, it is not the predominant conformation at a physiological pH of 7.2, due to the broadness of the experimentally observed distance distributions (Figures S2L–S2P). This

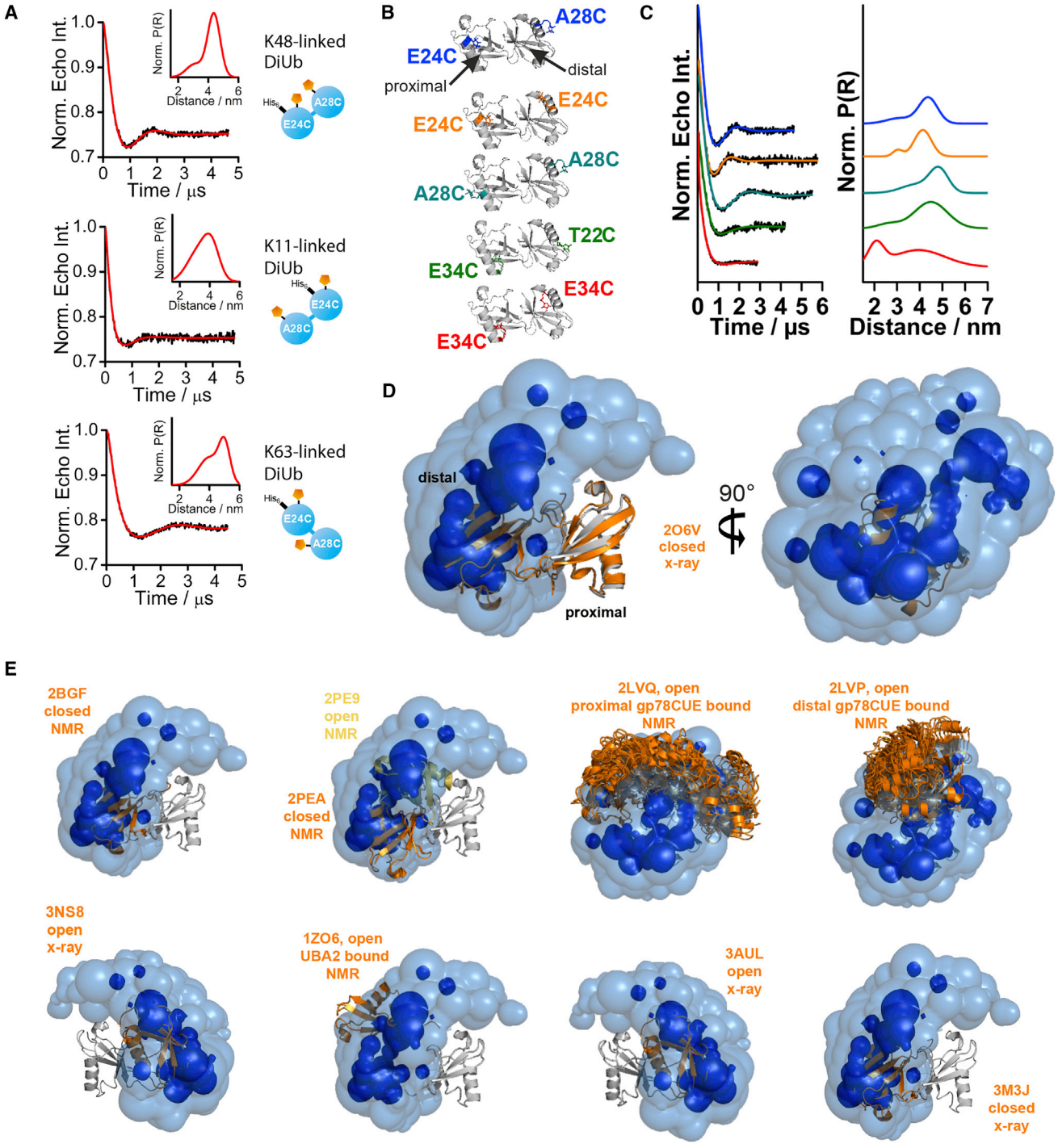

Figure 1. Analysis of the Conformational Space of K48-Linked Diubiquitin

(A) Conformational diversity of differently linked diubiquitin chains studied by PELDOR spectroscopy. Background-corrected four-pulse PELDOR time traces of K48-, K11-, and K63-linked diubiquitin chains labeled at position E24 in the proximal ubiquitin (E24C) and A28 in the distal ubiquitin (A28C). The resulting distance distributions were obtained from two-Gaussian model fitting and are shown as insets.

(B) Diubiquitin (PDB: 2PEA) mutants showing the labeling positions in the proximal and distal ubiquitin moieties.

(C) Background-corrected PELDOR time traces of doubly spin-labeled K48-linked diubiquitin chains and corresponding distance distributions obtained by two-Gaussian model fitting with the color code introduced in (B).

(D) Conformational ensemble obtained by CYANA of the distal ubiquitin moiety given for two combined probability cutoffs (light blue 0.12 and dark blue 0.4) with respect to the proximal moiety (gray). A closed conformation of diubiquitin is overlaid for comparison.

(E) Comparison of the conformational ensemble with available structures of free and bound diubiquitin. The distal ubiquitin of a certain structure is displayed in orange, whereas the proximal ubiquitin is aligned onto the reference proximal ubiquitin. In the case of diverse NMR structure ensembles all models are shown.

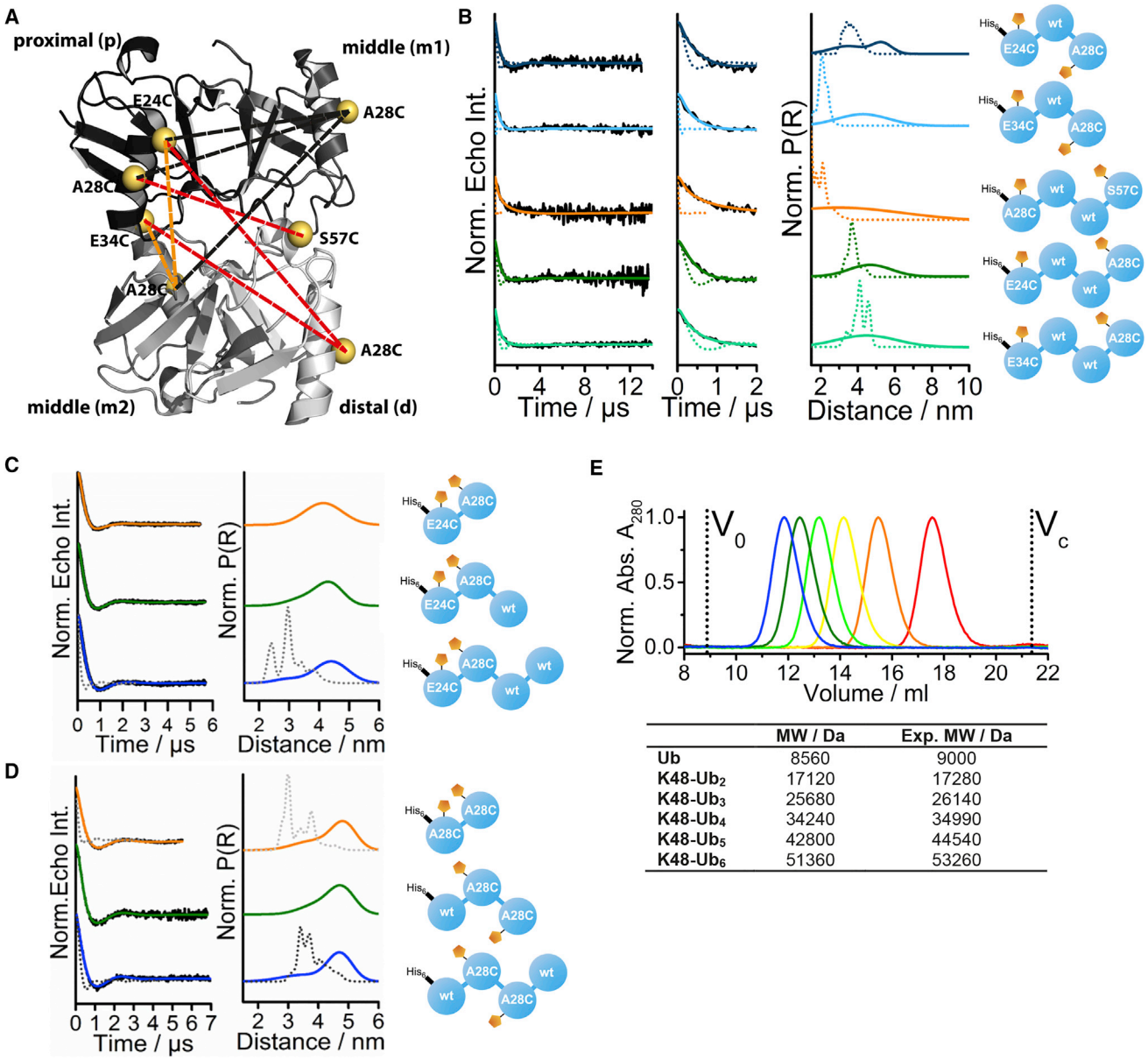

	MW / Da	Exp. MW / Da
Ub	8560	9000
K48-Ub$_2$	17120	17280
K48-Ub$_3$	25680	26140
K48-Ub$_4$	34240	34990
K48-Ub$_5$	42800	44540
K48-Ub$_6$	51360	53260

Figure 2. Conformational Flexibility of K48-Linked Ubiquitin Chains

(A) X-ray structure of tetraubiquitin (PDB: 2O6V) indicating the labeling positions in each ubiquitin moiety. Distances between directly adjacent ubiquitins are indicated in black, distances between Ub(i) and Ub(i + 2) in orange and Ub(i) and Ub(i + 3) in red.

(B) Left: seven-pulse CP PELDOR time traces of spin-labeled triubiquitin variants (pE24C/dA28C, blue; pE34C/dA28C, light blue) and for two tetraubiquitin variants (pA28C/dS57C, orange; pE24C/dA28C, green; pE34C/dA28C, cyan) in comparison with simulated dipolar evolution functions generated on the crystal structure of tetraubiquitin (PDB: 2O6V) (dotted lines); a zoom into early times of the dipolar evolution function is given as the inset. Right: corresponding distance distributions (solid lines) compared with the simulated distance distributions generated on the crystal structure of tetraubiquitin (PDB: 2O6V) (dotted lines). This reveals a broad conformational space for ubiquitin chains >3 moieties.

(C) The effect of an increasing chain length, as seen from four-pulse PELDOR time traces and distance distributions, on the conformational flexibility of K48-linked diubiquitin.

(D) Conformational flexibility of diubiquitin embedded in different positions in tri- and tetraubiquitin, revealing that any diubiquitin moiety behaves similar to free diubiquitin.

(E) Size-exclusion chromatography (SEC) profiles of wild-type K48-linked polyubiquitin chains and experimentally determined molecular weights compared with calculated molecular masses. SEC experiments were performed using a Superdex 75 10/300 GL column. Void volume (V_0) and column volume (V_c) are indicated.

interpretation is also consistent with measurements that show no difference between a diubiquitin unit in its free form and incorporated into a tri- or tetramer (Figures 2C, 2D, S2Q, S2R, and Movie S2). Likewise, data from tri- and tetraubiquitin chains labeled on ubiquitin 1 and 3 are virtually indistinguishable (Figures S2S–S2U). These results strongly suggest that the

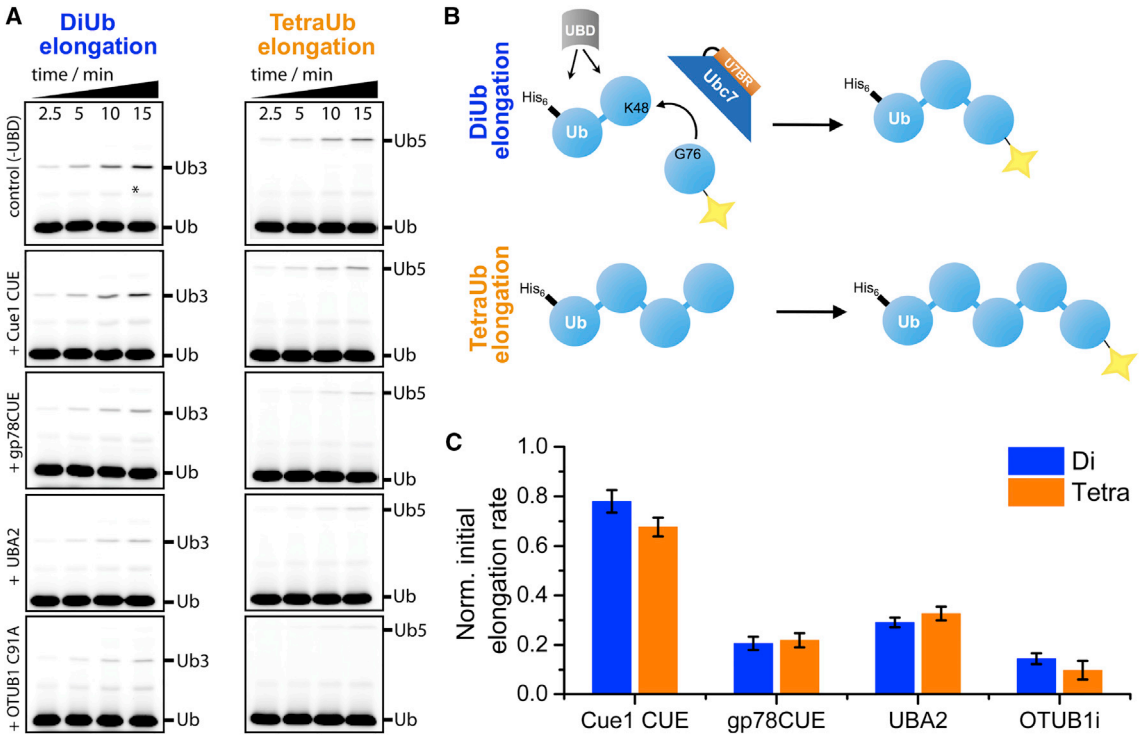

Figure 3. Impact of Ubiquitin Binding Proteins on Ubiquitin Chain Elongation by the E2 Enzyme Ubc7

(A) Fluorescence scan of SDS-PAGE-separated *in vitro* ubiquitin chain elongation reactions showing the substrate monoubiquitin as well as the reaction products (tri- or pentaubiquitin). Diubiquitin is indicated with an asterisk.

(B) Schematic depiction of the elongation assay used in (A). Preassembled K48-linked diubiquitin or tetraubiquitin chains were elongated by a single fluorescently labeled monoubiquitin using a complex of Ubc7 and its interacting region of Cue1 (U7BR). Different UBDs were added in excess during elongation.

(C) Quantification of the normalized initial elongation rates. Error bars represent the standard deviation calculated from performing experiments in triplicate.

conformation of K48-linked ubiquitin chains is determined by interactions between directly adjacent units with long-range interactions playing no significant role. However, we can also exclude that completely elongated chains contribute significantly to the conformational ensemble, since the length of such a conformation would be >10 nm. This interpretation is also consistent with size-exclusion chromatography experiments in which K48-linked ubiquitin chains showed elution volumes only slightly larger than globular proteins with the same molecular mass (Figure 2E), indicating that K48-linked chains are not fully elongated.

Ubiquitin Chain Elongation Is Differentially Affected by the Presence of Binding Proteins

In a previous study, we have shown that the CUE domain of Cue1 preferentially binds to the ubiquitin unit directly adjacent to the distal acceptor molecule of a substrate polyubiquitin (von Delbrück et al., 2016). Optimization of the entire reaction requires efficient recruitment of the growing chain to the E2 enzyme as well as the positioning and accessibility of K48 of the distal acceptor ubiquitin. In Cue1 this is achieved by positioning an E2 binding sequence (U7BR) for the E2 enzyme Ubc7 in *cis* to the CUE domain. While the recruitment of the ubiquitin chain is dependent on the affinity of the CUE domain, the positioning effect depends on the modulation of the conformational space of the ubiquitin chain. A high affinity of the CUE domain (significantly higher than the K_D of approximately 80 μM measured for binding of the CUE domain to the proximal position in ubiquitin chains; von Delbrück et al., 2016) could also inhibit the elongation process, similar to the preference of more closed conformations. To investigate the effect of the isolated CUE domain on the elongation efficiency, we measured "single" turnover elongation kinetics (Figures 3A and 3B). We found only small inhibitory effects of the CUE domain in the concentration range from 1:0.5 to 1:10 (ubiquitin chain:CUE domain). This suggests that based on its affinity and binding preference, the Cue1 CUE domain is optimally suited to accelerating the elongation process in an E4-like manner. In contrast, titrating the CUE domain of gp78, which has a higher affinity to ubiquitin, however, with a lower position preference within a chain, shows strong inhibitory effects. Likewise, the K48-selective UBA2 domain of Rad23a, which shows a preference for binding the K48-linkage between two ubiquitin moieties, also has a strong inhibitory effect (Figure 3C).

Conformational Selection of Ubiquitin Chains during Elongation

Guided by these results we investigated the impact of the Cue1 CUE domain on ubiquitin chain conformations to understand the elongation process within ERAD. We also investigated the effect of the human homolog gp78CUE (Liu et al., 2012) and the yeast homolog Cue2 (Kang et al., 2003), which have similar binding modes involving the hydrophobic patch (Husnjak and Dikic, 2012), and the UBA2 domain of Rad23a (Figure S3A). Notably,

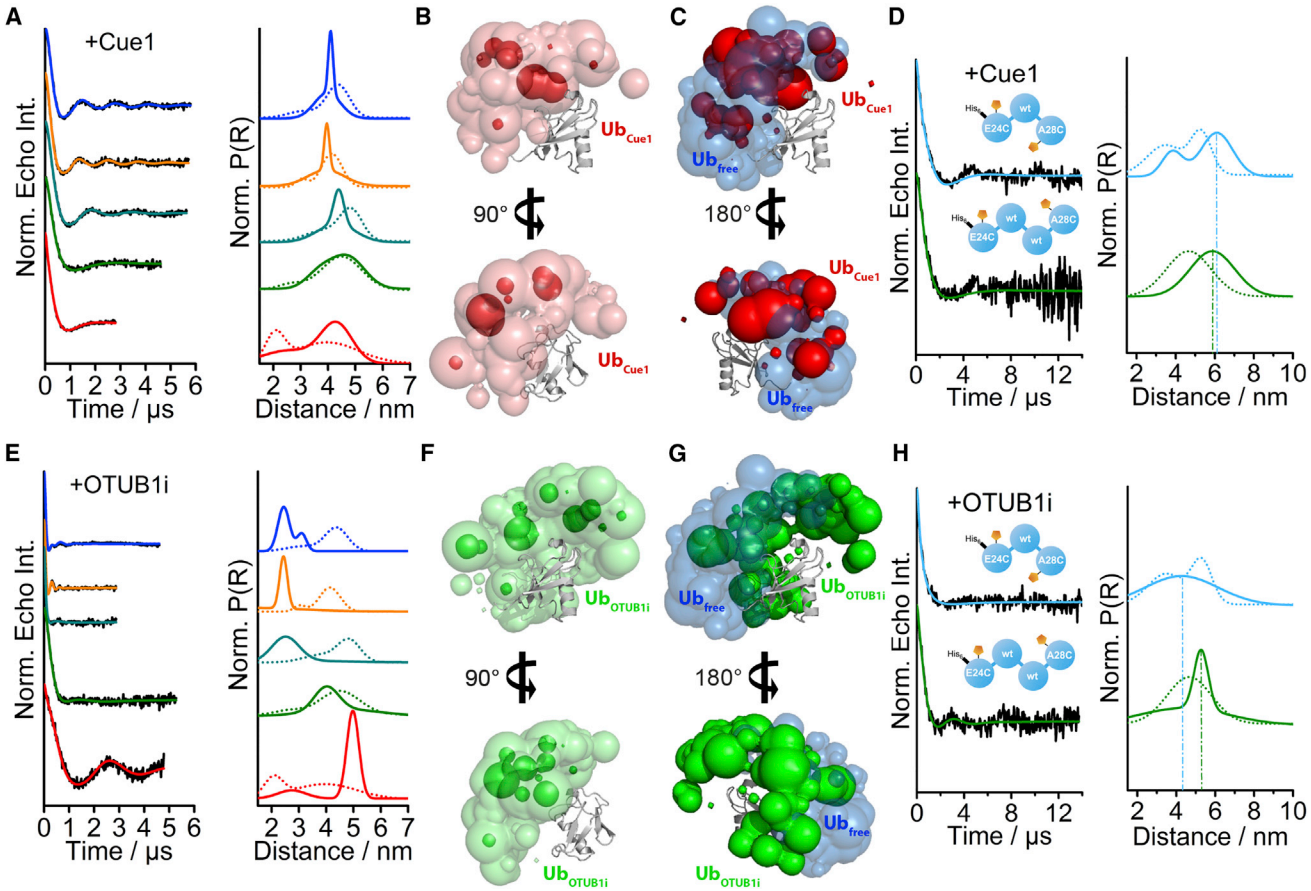

Figure 4. The Effect of the CUE Domain of Cue1 and the DUB OTUB1 on the Conformational Flexibility of Ubiquitin Chains

(A) Left: four-pulse PELDOR time traces of various doubly spin-labeled K48-linked diubiquitin chains in complex with the CUE domain of Cue1. Right: corresponding distance distributions of various doubly spin-labeled K48-linked diubiquitin chains in complex with the CUE domain of Cue1 (solid lines) in comparison with the free diubiquitin variants (dotted lines).

(B) Conformational ensemble of the distal ubiquitin moiety of diubiquitin in complex with Cue1 with respect to the proximal moiety (gray) given for two combined probability cutoffs (pink 0.12 and red 0.4).

(C) Comparison of the conformational ensemble of free (blue) and Cue1-bound (red) diubiquitin at a cutoff 0.2, indicating a conformational selection.

(D) Seven-pulse CP PELDOR time traces and corresponding distance distributions for doubly spin-labeled K48-linked tri- and tetraubiquitin chains in complex with the CUE domain of Cue1 (solid lines) in comparison with the free variants (dotted lines).

(E) Left: four-pulse PELDOR time traces of various doubly spin-labeled K48-linked diubiquitin chains in complex with OTUB1i. Right: corresponding distance distributions of various doubly spin-labeled K48-linked diubiquitin chains in complex with OTUB1i (solid lines) in comparison with the free diubiquitin variants (dotted lines).

(F) Conformational ensemble of the distal ubiquitin moiety of diubiquitin in complex with OTUB1i given for two combined probability cutoffs (light green 0.12 and dark green 0.4).

(G) Comparison of the conformational ensemble of free (blue) and OTUB1i-bound (green) diubiquitin at a cutoff 0.2, indicating a conformational remodeling of diubiquitin.

(H) Seven-pulse CP PELDOR time traces and corresponding distance distributions of tri- and tetraubiquitin chains in complex with OTUB1i (solid lines) in comparison with the free variant (dotted lines).

we observed the strongest effect for Cue1 (Figure S3A). Using our set of five spin-labeled diubiquitin molecules in complex with this CUE domain (Figures 4A, S3B, and S3C) allowed us to define the conformational space of K48-linked diubiquitin in this complex (Figures 4B and S3D). Comparison of the conformational distributions with free diubiquitin showed that the CUE domain restricts the conformational space and shifts it toward more open conformations (Figure 4C), demonstrating that the CUE domain of Cue1 uses conformational selection to bind to K48-linked diubiquitin (Movie S1). The selected highly populated open arrangements ensure accessibility of the distal acceptor lysine residue and may facilitate its positioning toward the E2 active site.

By introducing point mutations in both ubiquitin moieties to inhibit CUE domain binding (R42A) (von Delbrück et al., 2016), the observed conformational selection effect is completely abolished (Figure S3R). The same applies to mutations in the hydrophobic patch (V70A). Notably, these mutations, both located at the interface in closed K48-linked diubiquitin, had also a negligible effect on the PELDOR signal and distance distributions

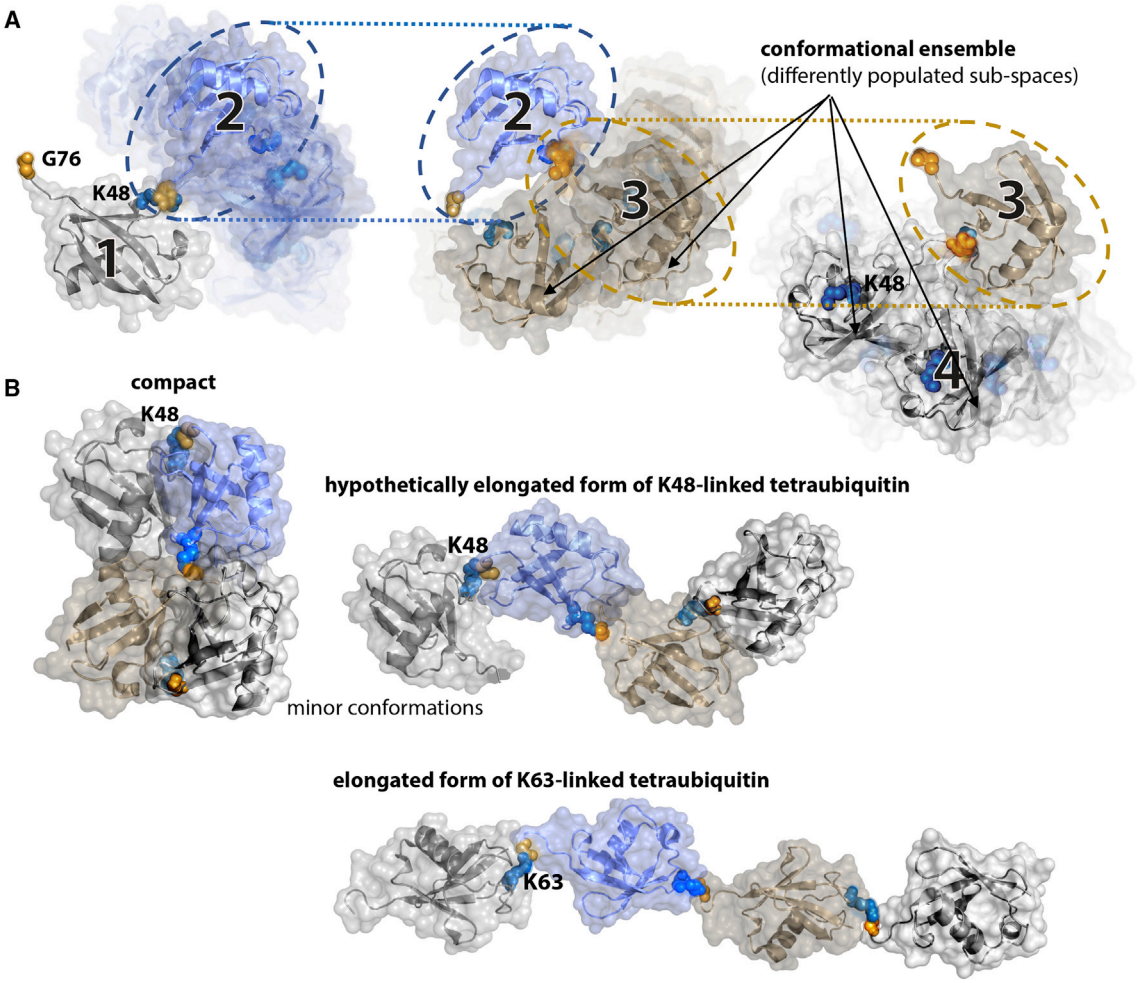

Figure 5. Model of the Conformational Distribution of K48-Linked Tetraubiquitin

(A) Schematic representation of the conformational space of K48-linked diubiquitin, which is characterized by distinctly populated sub-spaces. This specific conformational distribution seems to be largely independent of other neighboring ubiquitin molecules within a chain. One hypothetically highly populated conformer is elongated to triubiquitin thereby adding another layer of distinctly populated conformations to the overall conformational space of a chain. The same applies to the elongation to tetraubiquitin. Long-range interactions between not directly adjacent molecules as seen in the crystal structure of tetraubiquitin seem to be of only minor importance.

(B) The crystal structure of K48-linked tetraubiquitin (PDB: 2O6V), a hypothetical model of an elongated form of K48-tetraubiquitin, and the crystal structure of K63-linked tetraubiquitin (PDB: 3HM3). The specific arrangement of the conjugation sites (G76 and K48) makes it improbable to obtain a compact or a completely elongated conformation for K48-linked chains in solution. More likely K48-linked chains form a somewhat compact but dynamic arrangement of its ubiquitin molecules. By contrast, the K63-linkage allows formation of a completely elongated conformation as shown by the crystal structure of K63-linked tetraubiquitin.

obtained on free diubiquitin without the CUE domain. This further suggests that the conformational space of diubiquitin is not significantly impacted by specific inter-ubiquitin interactions.

For interaction of the Cue1 CUE domain with tri- and tetraubiquitin chains we observed a shift of the mean distance toward more elongated chains, however, without narrowing of the distance distribution (Figures 4D and S3E–S3I). This opening would be favorable for processes modifying chain length in the cellular context. Notably, for the homologous CUE domain gp78CUE, which is also involved in chain elongation, not only is the mean distance increased but also the distribution is broadened (Figures S3J–S3N). Similarly, the K48-linkage-specific UBA2 domain broadens the distance distributions of tetraubiquitin in combination with a shift toward a longer mean distance in accordance with a binding model where the linkage itself is recognized (Figures S3O–S3Q). These data show that the conformational distribution of tri- and tetraubiquitin is only slightly influenced by the CUE domain of Cue1, suggesting that the conformational selection by Cue1 is a local effect within the elongation processes probably restricted to the distal tip of a growing ubiquitin chain.

Conformational Remodeling of Ubiquitin Chains during Disassembly

As DUBs need direct access to the isopeptide bond connecting two ubiquitin moieties, their binding necessarily requires open conformations. Interestingly, the elongation assay revealed a strong inhibitory effect on chain elongation in the presence of an inactive mutant of the K48-linkage-specific Otubain protease

family member OTUB1 (OTUB1i) (Figure 3C). This indicates that open conformations do not necessarily stimulate chain elongation. On the basis of these data, we investigated the impact of OTUB1 on its respective substrate conformation. The interaction of OTUB1 with diubiquitin revealed a narrowing of three out of five distance distributions (Figures 4E and S4A). However, in contrast to the CUE domain, a shift to conformations that are less or even not populated in free diubiquitin was observed (Figures 4F, 4G, S4A, S4B, and Movie S1). A similar effect was observed for the inactivated mutant of the K11-linkage-specific DUB (OTUD7Bi) on K11-linked diubiquitin, suggesting that conformational remodeling may be a common mechanism of OTU domain-containing DUBs (Figure S4C). Addition of OTUB1i to K48-linked tri- and tetraubiquitin chains resulted in a conformational stabilization of tetraubiquitin leading to a narrower peak at 5.3 nm for ~40% of the overall population (Figures 4H and S4D–S4H; Table S1). This effect is most likely due to simultaneous binding of two DUBs to one tetraubiquitin chain.

DISCUSSION

Our data reported here suggest that K48-linked ubiquitin chains adopt a large conformational space that gets restricted either by conformational selection, as seen by interaction with UBDs such as the CUE domain, or by conformational remodeling, as seen by interaction with DUBs. Using five independently measured restraints allowed us to obtain a comprehensive view of the entire conformational space of ubiquitin chains and its modulation by interacting proteins. By contrast, calculation of a structural ensemble using a single restraint leads to differently populated distance distributions (Figure S1G). Our approach allows us not only to characterize the conformational space as a distribution between two or three distinct conformations but also to analyze all possible conformations and their population.

The sequential assembly of polyubiquitin signals by E2 enzymes is a spatially dynamic process, which would be strongly interfered by an inaccessible or sterically hindered distal acceptor lysine as occurring for compact conformations of K48-linked ubiquitin chains. In a previous investigation, we have shown that the CUE domain of Cue1 promotes chain elongation by orienting the distal tip of a ubiquitin chain relative to the E2 enzyme Ubc7. The selection of open/elongated polyubiquitin conformations is a prerequisite for efficient elongation. Using our PELDOR inter-moiety restraints we show that Cue1 uses conformational selection of a preexisting highly populated open conformation to support this elongation process.

The disassembly of K48-linked polyubiquitin chains is achieved by DUBs, such as OTUB1 (Juang et al., 2012; Wiener et al., 2012), which is an important regulatory aspect within the ubiquitination system. This processing requires direct access to the isopeptide linkage connecting neighboring ubiquitin moieties. Our PELDOR restraints in conjunction with structural modeling suggest a mechanism of conformational remodeling for proteolytic cleavage by OTUB1. This mechanism is evident by a shift of the conformational distribution toward weakly and even non-populated orientations within the DUB complexes. Such an interplay of conformational selection and remodeling to accomplish protein complex formation has been proposed earlier (Boehr et al., 2009; Ye et al., 2012).

In contrast to previous models, elongating the chain length from di- to tetraubiquitin does not restrict the conformational space to a closed and compact conformation but rather leads to a wider conformational distribution. This observation implies that no major structural rearrangement is required for proteasomal recognition and suggests that no new distinct structural motif is generated by the existence of a tetraubiquitin chain (Figure 5). In support of this model, investigation of the interaction of K48-linked diubiquitin with Rpn13 showed that the receptor induces a broader distribution of chain conformations (Figure S4I), suggesting that proteasomal recognition is based on the inherent conformational flexibility of ubiquitin chains. The high conformational flexibility ensures that concerted binding of the proteasomal receptors Rpn10 and Rpn13 is not inhibited. Electron microscopy studies have located these receptors on the proteasome approximately 10 nm apart (Sakata et al., 2012). This suggests that long and flexible chains are needed for a simultaneous and efficient binding of a ubiquitin chain to both receptors. This interpretation is consistent with recent findings that also (multi)monoubiquitinated proteins can be effectively degraded by the proteasome (Braten et al., 2016). In addition, there is no threshold length for a ubiquitin chain that constitutes a degradation signal (Lu et al., 2015). Combined with the lack of a tetraubiquitin-specific receptor these results also argue against a specific conformation that constitutes a degradation signal. However, the K48-linkage type produces a more compact arrangement of the ubiquitin units compared with K63-linked and linear chains, which are more extended (Figure 5). This arrangement might not be important for the initial binding to the proteasome but is relevant for the downstream processing.

STAR★METHODS

Detailed methods are provided in the online version of this paper and include the following:

- KEY RESOURCES TABLE
- CONTACT FOR REAGENT AND RESOURCE SHARING
- EXPERIMENTAL MODEL AND SUBJECT DETAILS
- METHOD DETAILS
  - Protein Purification
  - Preparative Assembly of Ubiquitin Chains
  - Spin Labeling
  - PELDOR Data Collection and Data Analysis
  - In Vitro Ubiquitin Chain Elongation for Fluorescence Based Analysis
  - Structure Ensemble Generation
  - Representation of the Ensemble Distribution as Probability Hyper-Surfaces
- QUANTIFICATION AND STATISTICAL ANALYSIS

SUPPLEMENTAL INFORMATION

Supplemental Information includes four figures, one table, and two movies and can be found with this article online at https://doi.org/10.1016/j.str.2017.12.011.

ACKNOWLEDGMENTS

This work was funded by the Deutsche Forschungsgemeinschaft (SFB 740, SFB 1177, Priority Program 1365, Priority Program 1601), the Deutsch-Israelische

Projektkooperation (DIP), the LOEWE (Landes-Offensive zur Entwicklung Wissenschaftlich-ökonomischer Exzellenz) program, Ubiquitin Networks (Ub-Net) of the State of Hessen (Germany), the Cluster of Excellence Frankfurt (Macromolecular Complexes), and the Center for Biomolecular Magnetic Resonance (BMRZ) at the Goethe University Frankfurt.

AUTHOR CONTRIBUTIONS

Conceptualization, A.K., D.S., T.S., T.F.P., and V.D.; Methodology, A.K., D.S., S.K., P.E.S. and L.P.; Investigation, A.K., D.S., S.K., L.P., K.H., and P.E.S.; Writing, A.K., D.S., S.K., T.S., T.F.P., and V.D.; Funding Acquisition, I.D., V.V.R., T.S., T.F.P., and V.D.; Resources, P.E.S., K.H., and P.G.; Supervision, I.D., V.V.R., P.G., T.S., T.F.P., and V.D. T.F.P. was responsible for the electron paramagnetic resonance spectroscopic parts and V.D. for the biochemical part and general conceptualization.

DECLARATION OF INTERESTS

The authors declare no competing interests.

Received: September 27, 2017
Revised: November 15, 2017
Accepted: December 19, 2017
Published: January 18, 2018

REFERENCES

Alfano, C., Faggiano, S., and Pastore, A. (2016). The ball and chain of polyubiquitin structures. Trends Biochem. Sci. *41*, 371–385.

Berndsen, C.E., and Wolberger, C. (2011). A spectrophotometric assay for conjugation of ubiquitin and ubiquitin-like proteins. Anal. Biochem. *418*, 102–110.

Boehr, D.D., Nussinov, R., and Wright, P.E. (2009). The role of dynamic conformational ensembles in biomolecular recognition. Nat. Chem. Biol. *5*, 789–796.

Braten, O., Livneh, I., Ziv, T., Admon, A., Kehat, I., Caspi, L.H., Gonen, H., Bercovich, B., Godzik, A., Jahandideh, S., et al. (2016). Numerous proteins with unique characteristics are degraded by the 26S proteasome following monoubiquitination. Proc. Natl. Acad. Sci. USA *113*, E4639–E4647.

Bremm, A., Freund, S.M., and Komander, D. (2010). Lys11-linked ubiquitin chains adopt compact conformations and are preferentially hydrolyzed by the deubiquitinase Cezanne. Nat. Struct. Mol. Biol. *17*, 939–947.

Dastvan, R., Brouwer, E.M., Schuetz, D., Mirus, O., Schleiff, E., and Prisner, T.F. (2016). Relative orientation of POTRA domains from cyanobacterial Omp85 studied by pulsed EPR spectroscopy. Biophys. J. *110*, 2195–2206.

Dikic, I., Wakatsuki, S., and Walters, K.J. (2009). Ubiquitin-binding domains - from structures to functions. Nat. Rev. Mol. Cell Biol. *10*, 659–671.

Dong, K.C., Helgason, E., Yu, C., Phu, L., Arnott, D.P., Bosanac, I., Compaan, D.M., Huang, O.W., Fedorova, A.V., Kirkpatrick, D.S., et al. (2011). Preparation of distinct ubiquitin chain reagents of high purity and yield. Structure *19*, 1053–1063.

Eddins, M.J., Varadan, R., Fushman, D., Pickart, C.M., and Wolberger, C. (2007). Crystal structure and solution NMR studies of Lys48-linked tetraubiquitin at neutral pH. J. Mol. Biol. *367*, 204–211.

Güntert, P., and Buchner, L. (2015). Combined automated NOE assignment and structure calculation with CYANA. J. Biomol. NMR *62*, 453–471.

Güntert, P., Mumenthaler, C., and Wüthrich, K. (1997). Torsion angle dynamics for NMR structure calculation with the new program Dyana. J. Mol. Biol. *273*, 283–298.

Hirano, T., Serve, O., Yagi-Utsumi, M., Takemoto, E., Hiromoto, T., Satoh, T., Mizushima, T., and Kato, K. (2011). Conformational dynamics of wild-type Lys-48-linked diubiquitin in solution. J. Biol. Chem. *286*, 37496–37502.

Husnjak, K., and Dikic, I. (2012). Ubiquitin-binding proteins: decoders of ubiquitin-mediated cellular functions. Annu. Rev. Biochem. *81*, 291–322.

Husnjak, K., Elsasser, S., Zhang, N., Chen, X., Randles, L., Shi, Y., Hofmann, K., Walters, K.J., Finley, D., and Dikic, I. (2008). Proteasome subunit Rpn13 is a novel ubiquitin receptor. Nature *453*, 481–488.

Jeschke, G. (2012). DEER distance measurements on proteins. Annu. Rev. Phys. Chem. *63*, 419–446.

Jeschke, G. (2013). Conformational dynamics and distribution of nitroxide spin labels. Prog. Nucl. Magn. Reson. Spectrosc. *72*, 42–60.

Jeschke, G., Chechik, V., Ionita, P., Godt, A., Zimmermann, H., Banham, J., Timmel, C.R., Hilger, D., and Jung, H. (2006). DeerAnalysis2006-a comprehensive software package for analyzing pulsed ELDOR data. Appl. Magn. Reson. *30*, 473–498.

Juang, Y.C., Landry, M.C., Sanches, M., Vittal, V., Leung, C.C., Ceccarelli, D.F., Mateo, A.R., Pruneda, J.N., Mao, D.Y., Szilard, R.K., et al. (2012). OTUB1 co-opts Lys48-linked ubiquitin recognition to suppress E2 enzyme function. Mol. Cell *45*, 384–397.

Kang, R.S., Daniels, C.M., Francis, S.A., Shih, S.C., Salerno, W.J., Hicke, L., and Radhakrishnan, I. (2003). Solution structure of a CUE-ubiquitin complex reveals a conserved mode of ubiquitin binding. Cell *113*, 621–630.

Klose, D., Klare, J.P., Grohmann, D., Kay, C.W., Werner, F., and Steinhoff, H.J. (2012). Simulation vs. Reality: a comparison of in silico distance predictions with DEER and FRET measurements. PLoS One *7*, e39492.

Komander, D., Clague, M.J., and Urbé, S. (2009). Breaking the chains: structure and function of the deubiquitinases. Nat. Rev. Mol. Cell Biol. *10*, 550–563.

Liu, S., Chen, Y., Li, J., Huang, T., Tarasov, S., King, A., Weissman, A.M., Byrd, R.A., and Das, R. (2012). Promiscuous interactions of gp78 E3 ligase CUE domain with polyubiquitin chains. Structure *20*, 2138–2150.

Lu, Y., Lee, B.H., King, R.W., Finley, D., and Kirschner, M.W. (2015). Substrate degradation by the proteasome: a single-molecule kinetic analysis. Science *348*, 1250834.

Mansour, W., Nakasone, M.A., von Delbruck, M., Yu, Z., Krutauz, D., Reis, N., Kleifeld, O., Sommer, T., Fushman, D., and Glickman, M.H. (2015). Disassembly of Lys11 and mixed linkage polyubiquitin conjugates provides insights into function of proteasomal deubiquitinases Rpn11 and Ubp6. J. Biol. Chem. *290*, 4688–4704.

Mevissen, T.E., Hospenthal, M.K., Geurink, P.P., Elliott, P.R., Akutsu, M., Arnaudo, N., Ekkebus, R., Kulathu, Y., Wauer, T., El Oualid, F., et al. (2013). OTU deubiquitinases reveal mechanisms of linkage specificity and enable ubiquitin chain restriction analysis. Cell *154*, 169–184.

Milov, A.D., Ponomarev, A.B., and Tsvetkov, Y.D. (1984). Electron-electron double-resonance in electron-spin echo - model biradical systems and the sensitized photolysis of decalin. Chem. Phys. Lett. *110*, 67–72.

Milov, A.D., Salikhov, K.M., and Shirov, M.D. (1981). Use of the double resonance in electron-spin echo method for the study of paramagnetic center spatial distribution in solids. Fizika Tverdogo Tela *23*, 975–982.

Pannier, M., Veit, S., Godt, A., Jeschke, G., and Spiess, H.W. (2000). Dead-time free measurement of dipole-dipole interactions between electron spins. J. Magn. Reson. *142*, 331–340.

Pickart, C.M., and Raasi, S. (2005). Controlled synthesis of polyubiquitin chains. Methods Enzymol. *399*, 21–36.

Polyhach, Y., Bordignon, E., and Jeschke, G. (2010). Rotamer libraries of spin labelled cysteines for protein studies. Phys. Chem. Chem. Phys. *13*, 2356–2366.

Rogov, V.V., Rozenknop, A., Rogova, N.Y., Lohr, F., Tikole, S., Jaravine, V., Guntert, P., Dikic, I., and Dotsch, V. (2012). A universal expression tag for structural and functional studies of proteins. Chembiochem *13*, 959–963.

Ryabov, Y., and Fushman, D. (2006). Interdomain mobility in di-ubiquitin revealed by NMR. Proteins *63*, 787–796.

Sakata, E., Bohn, S., Mihalache, O., Kiss, P., Beck, F., Nagy, I., Nickell, S., Tanaka, K., Saeki, Y., Förster, F., et al. (2012). Localization of the proteasomal ubiquitin receptors Rpn10 and Rpn13 by electron cryomicroscopy. Proc. Natl. Acad. Sci. USA *109*, 1479–1484.

Spindler, P.E., Waclawska, I., Endeward, B., Plackmeyer, J., Ziegler, C., and Prisner, T.F. (2015). Carr–Purcell pulsed electron double resonance with shaped inversion pulses. J. Phys. Chem. Lett. *6*, 4331–4335.

Spindler, P.E., Zhang, Y., Endeward, B., Gershernzon, N., Skinner, T.E., Glaser, S.J., and Prisner, T.F. (2012). Shaped optimal control pulses for increased excitation bandwidth in EPR. J. Magn. Reson. *218*, 49–58.

Thrower, J.S., Hoffman, L., Rechsteiner, M., and Pickart, C.M. (2000). Recognition of the polyubiquitin proteolytic signal. EMBO J. *19*, 94–102.

von Delbrück, M., Kniss, A., Rogov, V.V., Pluska, L., Bagola, K., Lohr, F., Guntert, P., Sommer, T., and Dotsch, V. (2016). The CUE domain of Cue1 aligns growing ubiquitin chains with Ubc7 for rapid elongation. Mol. Cell *62*, 918–928.

Wiener, R., Zhang, X., Wang, T., and Wolberger, C. (2012). The mechanism of OTUB1-mediated inhibition of ubiquitination. Nature *483*, 618–622.

Ye, Y., Blaser, G., Horrocks, M.H., Ruedas-Rama, M.J., Ibrahim, S., Zhukov, A.A., Orte, A., Klenerman, D., Jackson, S.E., and Komander, D. (2012). Ubiquitin chain conformation regulates recognition and activity of interacting proteins. Nature *492*, 266–270.

Zhang, Y., Vuković, L., Rudack, T., Han, W., and Schulten, K. (2016). Recognition of poly-ubiquitins by the proteasome through protein refolding guided by electrostatic and hydrophobic interactions. J. Phys. Chem. B *120*, 8137–8146.

STAR★METHODS

KEY RESOURCES TABLE

REAGENT or RESOURCE	SOURCE	IDENTIFIER
Bacterial and Virus Strains		
T7 Express Competent *E. coli* (High Efficiency)	New England BioLabs	CAT. # C2566H
Chemicals, Peptides, and Recombinant Proteins		
(1-Oxyl-2,2,5,5-tetramethylpyrroline-3-methyl) methanethiosulfonate (MTS) spin label (MTSSL)	Santa Cruz Biotechnology	CAT. # sc-208677
Alexa Fluor™ 488 C_5 Maleimide	ThermoFisher Scientific	CAT. # A10254
Recombinant DNA		
Human Ub (and its variants) in pETM60	this paper	N/A
Human Ub with C-terminal His6-tag (and its variants) in pETM60	this paper	N/A
Cdc34 in pGEX6p1	von Delbrück et al., 2016	N/A
Ubc13 in pGEX6p1	von Delbrück et al., 2016	N/A
Uev1a in pGEX6p1	von Delbrück et al., 2016	N/A
Ube1 in pET21d	Berndsen and Wolberger, 2011	N/A
pOPINK-OTUB1 (full-length, aa 1-271)	addgene	addgene Plasmid #61420
pOPINK-Cezanne (OTU, aa 53-446)	addgene	addgene Plasmid #61581
Cue1 CUE (aa 45-115) in pET39b(+)	von Delbrück et al., 2016	N/A
gp78CUE (aa 453-503) in pET39b(+)	von Delbrück et al., 2016	N/A
Cue2 CUE1 (aa 6-54) in pET39b(+)	von Delbrück et al., 2016	N/A
Ubc7 (aa 1-165) and Cue1 (aa 147-203, C147S) connected via a GG-linker in pET39b(+)	this paper	N/A
Ube2SΔC (aa 1-156) with C-terminal TEV cleavable His6-tag	this paper	N/A
Mouse Rpn13 (aa 1-150) cloned with an N-terminal His6-tag followed by a 3C protease cleavage site	Husnjak et al., 2008	N/A
Software and Algorithms		
MATLAB R2015b	The MathWorks Inc.	N/A
DeerAnalysis 2016 software package	Jeschke et al., 2006	http://www.epr.ethz.ch/software/deer-analysis-older-version.html
MMM2015.1 software package	Polyhach et al., 2010	http://www.epr.ethz.ch/software/mmm-older-versions.html
CYANA 3.9	Güntert et al., 1997 Güntert and Buchner, 2015	http://www.bpc.uni-frankfurt.de/guentert/wiki/index.php/Software
PyMOL 1.7.2.0	Schrödinger, LLC.	www.pymol.org
Other		
HisTrap FF, 5mL	GE Healthcare	CAT. # 17525501
HisTrap HP, 1mL	GE Healthcare	CAT. # 17524701
HiLoad 16/600 Superdex 75 pg	GE Healthcare	CAT. # 28989333
Superdex 75 10/300 GL	GE Healthcare	CAT. # 17517401
Mono S 5/50 GL	GE Healthcare	CAT. # 17516801
ELEXSYS E580 EPR spectrometer	Bruker, Billerica, MA	N/A
Bruker PELDOR unit (E580-400U)	Bruker, Billerica, MA	N/A
SuperQ-FT accessory	Bruker, Billerica, MA	N/A
Bruker AmpQ 10 W amplifier	Bruker, Billerica, MA	N/A
custom-made pulse-forming unit	(Innovative Technical Systems, Inc. AWG 8200)	N/A

(*Continued on next page*)

Continued

REAGENT or RESOURCE	SOURCE	IDENTIFIER
Bruker EN5107D2 resonator	Bruker, Billerica, MA	N/A
continuous-flow helium cryostat (CF935)	Oxford Instruments (Abingdon, UK)	N/A
temperature control system (ITC 502)	Oxford Instruments (Abingdon, UK)	N/A
150 W Q-band TWT	Bruker, Billerica, MA	N/A
Bruker AWG	Bruker, Billerica, MA	N/A
Q-Band Suprasil EPR Tubes (1.6*1.1.100 R/B)	Wilmad LabGlass an SP Intdustries Vompany	CAT. # WG-222-RB

CONTACT FOR REAGENT AND RESOURCE SHARING

Further information and requests for resources and reagents should be directed to and will be fulfilled by the Lead Contact, Volker Dötsch (vdoetsch@em.uni-frankfurt.de).

EXPERIMENTAL MODEL AND SUBJECT DETAILS

Expression of all proteins was performed in T7 Express Competent *E. coli* (New England BioLabs). Cells were grown in Terrific broth (TB) medium and induced at 18°C for 20h with 0.5 mM isopropyl-β-D-1-thiogalactopyranoside (IPTG) before harvest.

The following antibiotics were used for selection: 50 mg/mL kanamycin or 100 mg/mL ampicillin.

For cloning and plasmid preparations, E. coli DH5α was used. This strain was grown in LB medium at 37°C until saturation.

METHOD DETAILS

Protein Purification

Human ubiquitin and all its cysteine containing variants, cloned into pETM60, were expressed in T7 Express Competent *E. coli* cells (NEB) and purified as described elsewhere (Pickart and Raasi, 2005; von Delbrück et al., 2016). Enzymes for K48- and K63-linked chain synthesis Cdc34, Ubc13, Uev1a, cloned into pGEX6p1 vector, were expressed and purified as described before (Mansour et al., 2015). Ube1 sub cloned in a pET21d vector was expressed and purified as described by (Berndsen and Wolberger, 2011).

His6-GST tagged OTUB1 C91A (OTUB1i) and OTUD7B (Cezanne) (53-446, C194S) were expressed as previously described (Mevissen et al., 2013).

Codon-optimized synthetic genes of the Cue1 CUE domain (aa 45-115), gp78CUE (aa 453-503), Cue2 CUE1 domain (aa 6-54) and a single chain construct of Ubc7 (aa 1-165) and the U7BR of Cue1 (aa 147-203, C147S) connected via a GG-linker were expressed as TEV cleavable His10-tagged ubiquitin fusion proteins (Rogov et al., 2012). Ube2SΔC (aa 1-156), a c-terminally truncated version of human Ube2S (for K11-linked chain synthesis), was expressed containing a c-terminal tobacco etch virus (TEV) protease cleavage site followed by a hexahistidine tag. Mouse Rpn13 (aa 1-150) was expressed with an N-terminal His6-tag followed by a 3C protease cleavage site. Briefly, all expressions were carried out in T7 Express competent *E. coli*. Cells were grown in TB medium and induced at 18°C for 20h with 0.5 mM isopropyl-β-D-1-thiogalactopyranoside (IPTG). Purification was achieved by immobilized metal chelate affinity chromatography (IMAC), tag removal by TEV (except for Cue2 CUE1), a reversed IMAC step, followed by size exclusion chromatography using a HiLoad Superdex S75 column (GE Healthcare).

Preparative Assembly of Ubiquitin Chains

Proximally hexahistidine tag (6His) capped cysteine containing ubiquitin chains were enzymatically assembled *in vitro* as previously described (von Delbrück et al., 2016). K48-linkages were synthesized using Cdc34, K63-linked chains were generated by Ubc13 and Uev1a and K11-linkages were introduced using Ube2SΔC (aa 1-156) (Dong et al., 2011). To avoid contaminating K63- linkages during K11 chain synthesis all cysteine containing ubiquitin variants additionally contained a K63R mutation. Assembly of tri- and tetraubiquitin chains for PELDOR experiments required an iterative chain assembly protocol, where the desired reaction products were purified (by NiNTA purification and subsequent gel filtration) and reemployed in further preparative chain elongation reactions.

Wild type K48-linked chains of defined length for SEC experiments were synthesized in a single 20 mL reaction using 1 μM E1, 10 μM Cdc34, 1500 μM wild type Ub in buffer containing 50 mM Tris (pH 7.8), 20 mM ATP, 0.9 mM DTT, 9 mM $MgCl_2$ at 37°C overnight. Ub chains were diluted in 50 mM ammonium acetate (pH 4.5), filtered through a 0.2 μm syringe filter, applied in aliquots onto a MonoS column (GE Healthcare) and eluted using a salt gradient with 0.5 M NaCl as target concentration. Peak fractions were further purified using a 16/60 Superdex 75 gel filtration column.

Spin Labeling

Cysteine containing ubiquitin chains (100 μM) were labelled with 20-fold excess over the cysteine amount of (1-Oxyl-2,2,5,5-tetramethylpyrroline-3-methyl) methanethiosulfonate (MTS) spin label (MTSSL) in 1x PBS buffer for 1h at room temperature. Unreacted

MTSSL was removed using Amicon Ultra centrifugal filter units and buffer exchanged to deuterated PBS buffer (pD 7.2). 20% d8-glycerol was added as a cryoprotectant prior to flash freezing in liquid nitrogen. A labeling efficiency of 70% or higher was determined using CW EPR of the doubly spin-labeled polyubiquitin chain. This is in good agreement with modulation depth observed by PELDOR spectroscopy.

PELDOR Data Collection and Data Analysis

Pulsed EPR data were measured at Q-band frequencies (33.7 GHz) on an ELEXSYS E580 EPR spectrometer (Bruker, Billerica, MA) equipped with a Bruker PELDOR unit (E580-400U) and a SuperQ-FT accessory as well as a Bruker AmpQ 10 W amplifier and a Bruker EN5107D2 resonator. The temperature was kept at 50 K with a continuous-flow helium cryostat (CF935) and temperature control system (ITC 502), both from Oxford Instruments (Abingdon, UK). For PELDOR experiments the dead-time free four-pulse- or seven-pulse Carr-Purcell-PELDOR (CP PELDOR) sequences (Pannier et al., 2000; Spindler et al., 2015) were used. For the four-pulse sequence, typical pulse lengths were 32 ns ($\pi/2$ and π) for the probe pulses and 20 ns (π) for the pump pulse. The delay between the first and second probe pulses was varied between 260 and 372 ns or 136 248 in 8 ns steps, to reduce contributions from nuclear modulations. The shot repetition time was 4.5-5 ms. Four-pulse PELDOR measurements on triubiquitin variant mA28C/dA28C and tetraubiquitin variant m1A28C/m2A28C as well as diubiquitin variants in complex with Rpn13 were accomplished using a 150 W Q-band TWT. The pulse lengths were 32 ns ($\pi/2$ and π) for the probe pulses and 12 ns (π) for the pump pulse. The delay between the first and second probe pulses was varied between 260 and 372 in 8 ns steps, to reduce contributions from nuclear modulations. The shot repetition time was 4.5-5 ms. In terms of the seven-pulse Carr-Purcell (CP) sequence typical pulse lengths were 32 ns ($\pi/2$ and π) for the probe pulses and 400 ns (π) for the sech/tanh pump pulses. Using interpulse delays for the detection sequence according to (Spindler et al., 2015) were t1= 5000 ns, t2=10400 ns and t3= 10200 ns with an initial pump pulse positions T1= 232 ns, T2= 300 ns and T3= -232 ns, incremented with $\Delta1 = 24$ ns, $\Delta2 = 0$, $\Delta3 = -24$ ns. The sech/tanh pump pulses were generated with a homebuilt pulse shaping unit (Spindler et al., 2012). The carrier frequency of the pump pulses was matched to the resonance frequency of the resonator to ensure best inversion efficiency. In terms of the measurements on tri- and tetraubiquitin variants pE34C/dA28C and triubiquitin variant pE24C/m2A28C a 150 W Q-band TWT and the Bruker AWG (0.625 ns resolution) were used. For both experimental setups a 0, 180° phase cycle on the $\pi/2$-pulse was applied. The shot repetition time was 3 ms. The length of the PELDOR time trace evolution was chosen depending on the transversal relaxation time (Tm) of the samples. The frequency of the pump pulse was set to the max of the over-coupled resonator (Q ~300) and the magnetic field was adjusted, such that the excitation coincides with the maximum of the nitroxide powder spectrum (four-pulse) or the resonance frequency of the resonator (seven-pulse) to obtain maximum pumping efficiency. The probe frequency was chosen 70 MHz lower for both four-pulse and seven-pulse CP PELDOR. Seven pulse data was processed with a self-consistent iterative correction procedure (Spindler et al., 2015) to remove dipolar signal originating from the combinations of only one or two pump pulses. The probability of double spin inversion p was found to be ~0.72 (Spindler et al., 2015). A singly spin-labeled diubiquitin variant pE24C was produced to unravel the background decay of the seven-pulse CP PELDOR data. (Figure S2A) The PELDOR time traces were corrected for background decay using a homogeneous three-dimensional spin distribution. To obtain the distribution of distances between the spin labels, the background-corrected time domain PELDOR signals were processed using the DeerAnalysis2016 software package (Jeschke et al., 2006). *In silico* spin labeling of the ubiquitin and poly-ubiquitin structures (Protein Data Bank [PDB] codes: 2PEA, 2PE9, 2O6V, 3M3J, 1ZO6, 2IVQ, 2LVP, 1AAR, 2BGF, 3AUL, 3NS8) using rotamer library approach and estimation of interspin distances were performed using the MMM 2015.2 software package in 298 K mode (Polyhach et al., 2010).

In Vitro Ubiquitin Chain Elongation for Fluorescence Based Analysis

In vitro ubiquitination reactions (performed in triplicates) for the analysis of ubiquitin chain elongation kinetics included 0.1 μM E1, 2 μM of a single chain construct (Ubc7U7BR) comprising the E2 Ubc7 and the Ubc7 interacting region of Cue1 (U7BR, $Cue1^{147\text{-}203,\ C147S}$), 10 μM preassembled c-terminally hexahistidine tagged ubiquitin chains, 1 μM Alexa Fluor 488-labelled Ub and 20 μM (for diubiquitin elongation) or 40 μM (for tetraubiquitin elongation) of various UBDs. The reactions were carried out at 30°C in buffer containing 50 mM Tris (pH 7.5), 2.5 mM $MgCl_2$, 4mM ATP, 0.5 mM DTT. At indicated time points the reaction was stopped by addition of SDS sample buffer and elongation products were analyzed by SDS-PAGE following fluorescence scanning employing emission filter LPB (510LP) after excitation at 473 nm.

Structure Ensemble Generation

In the first step, an ensemble of diubiquitin structures with a broad distance distribution between the monomers was generated using CYANA 3.9 (Güntert and Buchner, 2015; Güntert et al., 1997). To do so a CYANA library entry for the spin label MTSSL was generated. To include the EPR distance restraints into the structure calculations, this entry includes a virtual atom (without any interaction to other atoms) placed in the center of the terminal N-O bond to represent the unpaired electron and serves to define the PELDOR distance restraint between the virtual atoms of a spin label pair. Unlike in the experiments where only one spin pair in each probe was present, in the structure calculation spin labels were inserted at all positions (residue T22, E24, A28, and E34) in both monomers for which an experimental distance distribution was measured. During all calculations, the backbone angles φ and ψ of the core ubiquitin residues (residues 1 to 71) for both monomers were fixed to the values found in the first chain of the diubiquitin reference crystal structure (PDB: 2PEA). The flexible region (residues 72 to 76) and all side-chain χ angles move freely except the spin labels side-chains for which the conformations were restricted by a rotamer library generated by MMM2015.2 in 298 K mode (Polyhach et al., 2010) based

on the reference NMR structure (PDB: 2PEA). To include the rotamer library restraints for the specific residues an in-house developed extension of CYANA was used (Güntert and Buchner, 2015; Güntert et al., 1997). This approach allows CYANA to take into account the entire bundle of rotamers from the given rotamer library. This is realized by a new restraint that has a value of 0 (no contribution to the target function) if the spin label side-chain adopts a conformation included in the library and increases with increasing deviation from this library. After the calculation, this restraint was checked and structures with the rotamer restraint larger than a pre-defined threshold value were not further considered. Additionally, a modified lysine residue CYANA library entry was generated by deleting two of the hydrogens of the lysine's zeta nitrogen. This modified lysine was connected to the second monomer's c-terminal glycine by nine upper and lower limits with a thousand-fold weight to guarantee an optimal binding geometry. For each structure calculation five additional distances between the spin label pairs were set as described below.

To define entire conformation space allowed by the PELDOR measurements we extracted from these measurements both the minimal and the maximal distances. These were 1.5-5.1 nm, 1.9-5.2 nm, 1.5-5.7 nm, 3.0-5.8 nm, and 1.6-5.7 nm for the spin label pairs pE24C/dE24C, pE24C/dA28C, pA28C/dA28C, pE34C/dT22C, and d34C/dE34C, respectively. Using these five distance ranges we created a conformational ensemble by systematically varying each distance range separately in steps of 0.5 ±0.25 nm (e.g. 2.75 nm as lower and 3.25 nm as upper bound for a distance of 3 nm). Thus, this conformational ensemble contains all possible combinations of five distances within each of these distance ranges. Overall 51,001 structure calculations were performed. For each distance combination, a bundle of 20 structures with the lowest target function out of 100 calculated structures was generated. All structures showing van der Waals collisions between the two ubiquitin chains or not fulfilling the above described distance restraints were dropped to generate a collision-free conformational ensemble of $\sim 3.7 \times 10^5$ models. This ensemble represents the accessible conformational space that is consistent with the upper and lower boundaries of the PELDOR measurements.

To calculate the population distribution within this conformational space each conformation of this ensemble was weighted by a pseudo probability. Taking the PELDOR distance distribution as a density distribution (with an integral of unity) we calculated a combined probability factor for any given structure. The height of the PELDOR distance distribution was used as a pseudo probability for each distance. For any given structure, we multiplied all five pseudo probabilities to obtain an overall probability factor. The resulting values for each structure were afterwards divided by the maximum probability obtained in these calculations such that the structure with the highest value is assigned the probability of one. This creates a relative pseudo probability that allows us to compare the relative weights of specific conformations. Hereafter, all structures with a relative pseudo probability of less than 1% were dropped. This resulted in an ensemble of free K48-linked diubiquitin of $\sim 1.4 \times 10^5$ models, an ensemble of 4.1×10^4 models for diubiquitin in complex with Cue1 and an ensemble of 1.2×10^4 models for diubiquitin in complex with OTUB1i.

Representation of the Ensemble Distribution as Probability Hyper-Surfaces

To visualize the distribution of the distal ubiquitin relative to the proximal ubiquitin with respect to the assigned probabilities a three-dimensional grid was generated. The backbone atoms of the proximal ubiquitin (only residues 1 to 71 which were kept rigid in the calculation) were superimposed. For the representation a subset of 3000 structures that show the same probability distribution as the full set were selected. Each distal ubiquitin was represented as a truncated 3D Gaussian (Equation 1) around its geometric center (with coordinates C_{ix}, C_{iy}, C_{iz}).

$$G_i(x,y,z) = p_i \cdot e^{\frac{-(x-c_{ix})^2-(y-c_{iy})^2-(z-c_{iz})^2}{2 \cdot r_0^2}} \quad \text{(Equation 1)}$$

Each Gaussian with $r_0 = 3.5\ nm$ was scaled such that the maximum equals the probability pi of the specific structure. All values above a certain truncation radial distance of $r_0^2/2$ were set to zero in the grid. The grids containing Gaussians for each structure of the ensemble were merged into one grid by taking the maximum value of each grid-point. Showing hyper-surfaces covering regions above threshold values (as in three-dimensional contour lines) for this probability grid in PyMOL results in overlapping globes where the radius of each globe represents the probability of a representative conformation at this point.

QUANTIFICATION AND STATISTICAL ANALYSIS

In vitro ubiquitination reactions for the analysis of ubiquitin chain elongation kinetics were performed in triplicates (n=3).